Macroporosity and Grain Density of Rubble Pile Asteroid (162173) Ryugu

Matthias Grott[1], Jens Biele[2], Patrick Michel[3], Seiji Sugita[4], Stefan Schröder[1], Naoya Sakatani[5], Wladimir Neumann[6,1], Shingo Kameda[7], Tatsuhiro Michikami[8], Chikatoshi Honda[9]

[1]German Aerospace Center, Berlin, Germany
[2]German Aerospace Center, Cologne, Germany
[3]Université Côte d'Azur, Observatoire de la Côte d'Azur, CNRS, Laboratoire Lagrange, Nice, France
[4]University of Tokyo, Tokyo, Japan
[5]ISAS/JAXA, Sagamihara, Japan
[6]Klaus-Tschira-Labor für Kosmochemie, Institut für Geowissenschaften, Universität Heidelberg, Heidelberg, Germany
[7]Rikkyo University, Tokyo, Japan
[8]Kindai University, Hiroshima, Japan
[9]University of Aizu, Aizu-Wakamatsu, Japan

Key Points:

- Ryugu's large bulk porosity is distributed between intrinsic boulder microporosity and macroporosity due to void spaces in-between boulders.
- We use the boulder size-frequency distribution as observed on the surface together with mixing models to estimate Ryugu's macroporosity.
- We find that macroporosity is 16±3 %, indicating that Ryugu's large bulk porosity of close to 50 % is governed by microporosity.

Corresponding author: Matthias Grott, matthias.grott@dlr.de

Abstract

Rubble pile asteroids such as (162173) Ryugu have large bulk porosities, which are believed to result from void spaces in between the constituent boulders (macroporosity) as well as void spaces within the boulders themselves (microporosity). In general, both macroporosity and microporosity are estimated based on comparisons between the asteroid bulk density and both the bulk and grain density of meteorite analogues, and relatively large macroporosities are usually obtained. Here we use semi-empirical models for the macroporosity of multi-component mixtures to determine Ryugu's macroporosity based on the observed size-frequency distribution of boulders on the surface. We find that Ryugu's macroporosity can be significantly smaller than usually assumed, as the observed size-frequency distribution allows for an efficient packing of boulders, resulting in a macroporosity of 16 ± 3 %. Therefore, Ryugu's high bulk porosity must be a direct consequence of a very large boulder microporosity. Furthermore, using estimates of boulder microporosity around 48 % as derived from in-situ measurements, the average grain density in boulders is 2751 ± 236 kg m^{-3}, similar to values obtained for CM, CI, and the Tagish lake meteorites. Ryugu's bulk porosity corresponding to the above values is 57 %.

Plain Language Summary

The carbonaceous asteroid (162173) Ryugu formed from fragments which re-accreted after its parent body was disrupted by a catastrophic collision. Asteroids of this type are also known as rubble piles and the re-accumulation process is thought to be one of the causes for their large bulk porosity. We have applied mixing models to determine the amount of inter-boulder porosity taking the observed abundance of large and small boulders on the surface into account. We find that the relative abundances of differently sized boulders allow for a very efficient packing, such that inter-boulder porosity in Ryugu is rather small and only 16 ± 3 %. This implies that a large part of the estimated 50 % total porosity must reside inside the boulders themselves. Using estimates of boulder intrinsic porosity as derived from thermal infrared measurements, we furthermore constrain the average density of the boulder's constituent minerals to 2751 ± 236 kg m^{-3}, which is consistent with values measured for carbonaceous meteorites as collected on Earth. If Ryugu is representative of the carbonaceous asteroid population, inter-boulder porosity of rubble pile asteroids may have been systematically overestimated in the past.

1 Introduction

Upon arrival of the Hayabusa2 spacecraft the C-complex asteroid (162173) Ryugu was found to be a spinning top-shaped rubble pile (Watanabe et al., 2019) with Cb-type spectrum and very low albedo around 0.045, consistent with thermally metamorphosed CM/CI meteorites (Sugita et al., 2019). Observations further show that a weak 2.7 µm-absorption is present, suggesting a small amount of hydrated minerals to be present (Kitazato et al., 2019). Furthermore, the surface was found to be dominated by large blocks and boulders (Sugita et al., 2019; Michikami et al., 2019). A bulk density of 1190±20 kg m^{-3} was determined using the SFM20180804 shape model (Watanabe et al., 2019), which allowed for an estimate of asteroid porosity. Assuming typical grain densities for carbonaceous chondrites (Britt & Consolmagno S.J., 2001; Macke et al., 2011; Flynn et al., 2018), bulk porosity estimates close to 50 % are obtained (Watanabe et al., 2019), which is consistent with the bulk porosity estimates for C-complex asteroids.

The bulk porosity inside rubble pile asteroids can be separated into two contributions: the first one stems from the intrinsic porosity of rocks and boulders and is termed microporosity, while the second contribution refers to voids in-between particles and is termed macroporosity (Britt et al., 2002). The latter is directly related to the geometrical arrangement of the constituent blocks, also known as the packing state, and macroporosity of the average C-complex is estimated to be 25-30 % (Britt et al., 2002). This is generally consistent with models of the reassembly of blocks after a catastrophic disruption, which result in macroporosities of 20-40 % (Wilson et al., 1999). However, simulations suffer from unrealistically large lower cutoff sizes for the considered boulder population, such that lower macroporosities cannot be ruled out.

Little is known about the packing state of rubble pile asteroids following reaccretion, which depends on many parameters like, e.g., the distribution of angular momentum in the reaccreting system as well as the size distribution and shape of reaccreting fragments. Laboratory experiments on the disruption of monoliths (Nakamura & Fujiwara, 1991; Durda et al., 2015; Michikami et al., 2016) indicate that shattered particles have elongated shapes, and while large deviations from a spherical shape would reduce packing efficiency, results of disruption experiments need to be interpreted with caution, as the high strain rates imposed during the experiment may not be representative for the destruction of larger blocks. In general, small boulders on bodies such as Itokawa,

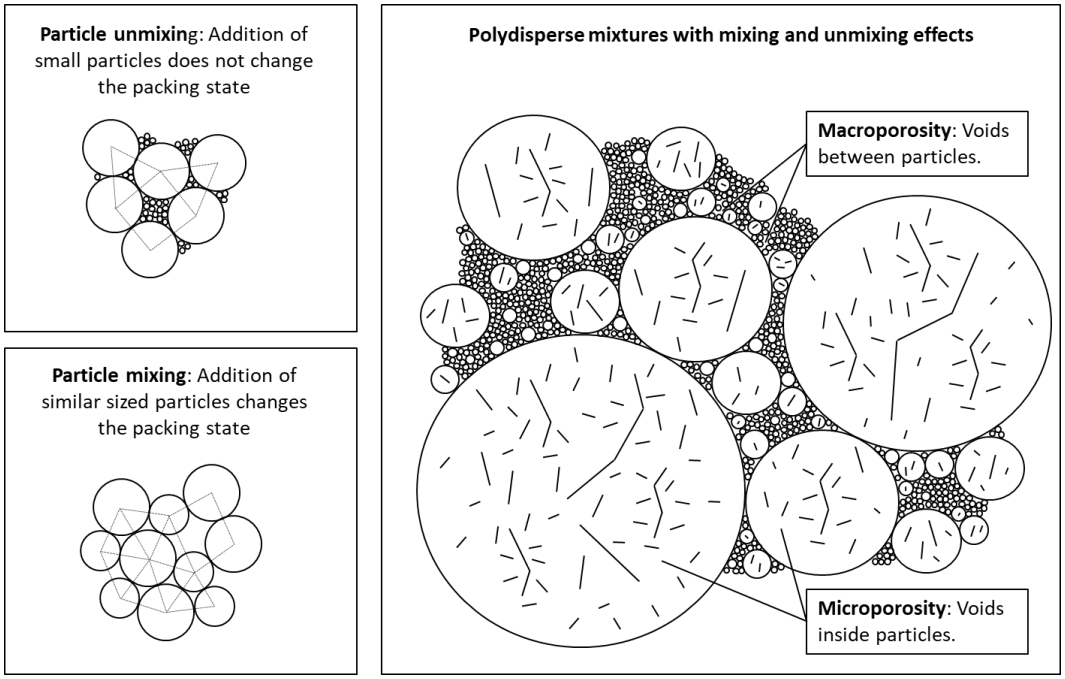

Figure 1. Top Left: Illustration of particle unmixing for particles with strongly disparate diameters. Bottom Left: Illustration of particle mixing for particles with similar diameters. Right: Two dimensional illustration of the random packing structure of strongly polydisperse spheres. As compared to monodispersed configurations, porosity is reduced by the filling of void spaces. Macroporosity refers to the porosity generated by the void spaces between particles, while microporosity is caused by void spaces and cracks that formed inside individual particles. Figure adapted from Yu & Zou (1998).

Bennu, and Ryugu are considered to be relicts of the direct formation of those asteroids by gravitational reaccumulation following the disruption of their parent bodies (Michel & Richardson, 2013; Michel et al., 2020) rather than the result of impact events after formation has been completed.

Here we investigate the macroporosity of asteroid Ryugu using semi-empirical models for the porosity of multi-component mixtures of non-spherical, cohesive particles (Zou et al., 2011). Such models predict the macroporosity of granular material given the particle shape as well as a particle size distribution applying linear mixing and using the concept of controlling mixtures (Yu & Standish, 1991) to calculate the packing state. In general, polydisperse particle mixtures can have a macroporosity which is considerably smaller than the canonical 36 % for a random close packing or 40 % for a random loose

packing of spherical, monosized particles (Scott, 1960), and values down to 10 % can be reached (Dullien, 1991).

In binary mixtures, the way particles interact depends on their size ratio, and if this ratio is less than 0.154 (Graton & Fraser, 1935), small particles will not affect the packing state and simply fill the gaps between larger ones. In contrast to this unmixing of particles, similar sized particles will mix, creating a new packing structure (also see Yu & Zou (1998) for a discussion of mixing and unmixing effects). Applying these concepts to polydisperse mixtures, particle unmixing will take place for very small and very large particles, as smaller particles start filling the gaps and larger particles completely fill some regions with solid material. The component controlling the porosity of the mixture is then defined by intermediate sized particles, which do not change their packing state by the addition of unmixing components (Yu & Zou, 1998). An illustration of particle mixing and unmixing is shown in Fig. 1.

The semi-empirical models by Yu & Zou (1998) and Zou et al. (2011) can be applied to particle mixtures in loose and dense packing states. They have been shown to reproduce the porosity of mixtures created using the funnel method, in which particles are carefully poured into a container, as well as the porosity of mixtures tapped many times to reach maximum compaction. As the initial packing state is a free parameter in the mixing theory, we will systematically vary it in the analysis below. It is worth noting, however, that the packing state of rubble pile asteroids like Ryugu is likely best represented by a random close packing structure, as meteoritic bombardment (Sugita et al., 2019) and seismic shaking will result in particle rearrangement and a reduction of pore spaces.

In order to apply the theory of multi-component mixtures, the shape and size distributions of boulders need to be known. Here we use the boulder size and shape distributions determined by Michikami et al. (2019), who extend the analysis in Sugita et al. (2019) using images from the Hayabusa2 optical navigation camera (ONC) which have near global coverage and were acquired at altitudes between 20 km and 6.5 km. These have spatial resolutions of up to 0.65 m/pixel, and smaller boulders, cobbles and pebbles with sizes of 0.02 to 9.1 m were studied using close-up images of the sample areas, where images taken at altitudes from 67 m to 620 m with resolutions down to < 0.01 m/pixel are available (Sugita et al., 2019). Overall, size-frequency and shape distribu-

tions were determined in the 0.02 to 140 m size range and we assume that the same distribution holds in the interior.

To estimate asteroid macroporosity from mass and volume as measured by spacecraft, some assumption on the average density of the constituent rocks and boulders needs to be made. Usually, densities of spectrally similar meteorite samples are assumed (Britt & Consolmagno S.J., 2001; Watanabe et al., 2019; Sugita et al., 2019), which effectively fixes the material's microporosity and grain density. In the special case of Ryugu, microporosity has been estimated from thermal inertia as determined in situ (Grott et al., 2019) and from orbit (Sugita et al., 2019; Okada et al., 2020), such that some constraints on the material's grain density can be derived based on the observation that the vast majority of boulders corresponds to the low thermal inertia type (Okada et al., 2020).

Therefore, we will in the following first introduce the theory of determining asteroid macro-porosity from a given size and shape distribution for the rocks and boulders. We will then derive a simple equation relating grain density to macro- and microporosity, and results of the macroporosity calculation and relevant uncertainties will then be used in a Monte-Carlo approach to estimate grain density of Ryugu's constituent material. Finally, results, assumptions, and implications will be discussed.

2 Methods

2.1 Particle Size and Shape Distributions

To estimate Ryugu's macroporosity or packing state, the constituent boulder's size and shape distributions need to be known. These were determined by Michikami et al. (2019) who fitted size-frequency data using power laws. Power law exponents between 1.65 and 2.65 were obtained, with 2.65 being the best fit for the global dataset. Furthermore, particles were generally found to be elongated, and axis ratios for boulders > 2 m are close to 0.70, consistent with boulder generation by impact processes (Michikami et al., 2019). The data provided by Michikami et al. (2019) can be adequately represented by a cumulative Weibull (Rosin-Rammler) distribution (Rosin & Rammler, 1933; Weibull, 1951; Wingo, 1989; Brown & Wohletz, 1995), and the cumulative size-frequency distribution $N(D)$ is then given by

$$N(D) = N_T e^{-3(D/\lambda)^\beta/\beta} \tag{1}$$

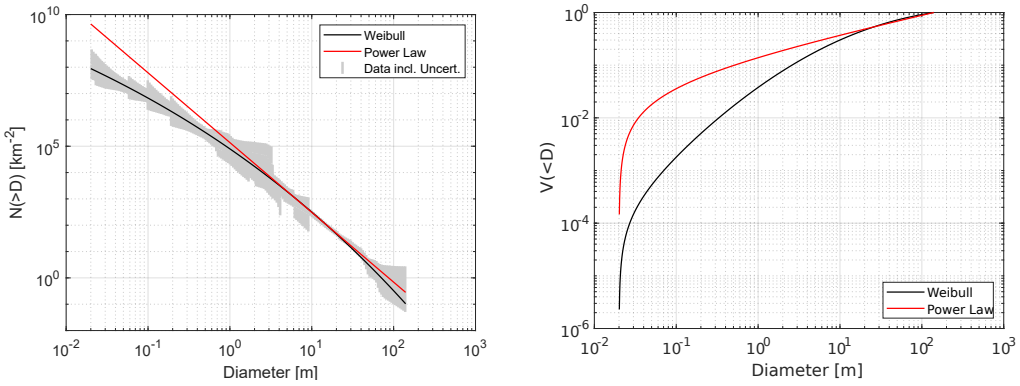

Figure 2. Left: Cumulative particle size frequency distribution (SFD) as derived for Ryugu by Michikami et al. (2019) in different size-bins. Our Weibull fit to the data (black) is shown along with a power law fit with exponent $p = 2.65$ (red). Right: Cumulative volume fraction distribution for the SFDs on the left hand side of the figure.

where D is the mean horizontal diameter, and we determined the fit parameters $\beta = 0.09495$, $\lambda = 33.78$ m, and $N_T = 5.28 \cdot 10^{14}$ km^{-2} by a weighted least-squares approach. The resulting distribution $N(D)$ is shown together with the uncertainty of the data in Fig. 2. It is worth noting that representing the data using a single power law for the entire size range does not adequately represent the data.

Given the size-frequency distribution $N(D)$ as determined from surface counts of boulders, the cumulative volume distribution $V(D)$ can be calculated by numerical integration. It is given by

$$V(D) = c\left(N_{\mathrm{tot}} D_{\mathrm{min}}^3 - N(D)D^3 + \int_{D_{\mathrm{min}}}^{D} N(D')3D'^2 dD'\right) \tag{2}$$

where N_{tot} is the total number of particles counted per unit area, D_{min} is the minimum particle size of the particle size distribution $N(D)$, and c is a normalization factor chosen such that $V(D_{\mathrm{max}}) = 1$.

In addition to the Weibull distribution fit to the data represented by Eq. 1, we will also consider a simple power law to systematically study the influence of the particle size distribution's power law exponent p on the obtained results. The distribution can then be expressed as

$$N(D) = N_{\mathrm{tot}} \left(D/D_{\mathrm{min}}\right)^{-p} \tag{3}$$

where $p = 2.65$ represents the best fit to the global dataset (Michikami et al., 2019). For the power law defined by Eq. 3, Eq. 2 can be integrated analytically and the volume size distribution is then given by

$$V(D) = \frac{D^{3-p} - D_{\min}^{3-p}}{D_{\max}^{3-p} - D_{\min}^{3-p}} \tag{4}$$

for $D_{\min} \leq D \leq D_{\max}$. For $D \geq D_{\max}$, $V(D) = 1$, whereas for $D \leq D_{\min}$ $V(D) = 0$.

Michikami et al. (2019) give the shape of boulders in terms of the maximum dimensions in three mutually orthogonal planes ($a \geq b \geq c$). Here we primarily regard the axis ratio b/a, with a being the maximum and b the intermediate dimension. As reported by Michikami et al. (2019), shape of particles on Ryugu appears to be largely independent of geographical longitude, whereas some dependence on latitude may indicate boulder migration. Nevertheless, average b/a is only weakly size-dependent and close to 0.71.

In general, particle sphericity is defined as the ratio of the surface area of a sphere (with the same volume as the particle) to the surface area of the particle (Wadell, 1932). However, this is difficult to evaluate in practice, and the Krumbein (Krumbein, 1941) or Riley (Riley, 1941) simplifications are usually applied. Working with two dimensional (image) data, we define sphericity Ψ as

$$\Psi = \sqrt{\frac{D_i}{D_c}} \tag{5}$$

where D_i is the diameter of the largest inscribed circle and D_c is the diameter of the smallest circumscribing circle for a given particle (Riley, 1941). Using Eq. 5, the shape parameter b/a derived by Michikami et al. (2019) then translates into a sphericity of $\Psi = 0.833 \pm 0.014$. In addition, Michikami et al. (2019) also estimated the third axis, c/a, of 121 arbitrarily selected boulders. The mean axes ratio c/a was found to be 0.44, and the sphericity of a parallelepiped with axis ratios a:b:c of 1:0.71:0.44 is 0.796. On the other hand, sphericity of a triaxial ellipsoid with the same axis ratios is 0.913. Therefore, sphericity depends not only on axis ratios, but also on particle shape, and we will use $\Psi = 0.85 \pm 0.06$ as an average sphericity in the following. It is worth noting that while sphericity is a second order effect for the packing model if it is independent of particle size and larger than 0.8 (which is the case studied here), it directly enters the calculation of the Bond number, which accounts for inter-particle forces (compare Eq. 14 below).

2.2 Macroporosity

The macroporosity of Ryugu can be calculated from the volume size-frequency distribution (Eq. 2) assuming linear mixing models (Yu & Zou, 1998; Zou et al., 2011). In the mixing theory, the macroporosity achieved by the particular size distribution will be a function of the volume fractions X_i, the initial porosity ϕ_i, as well as the nominal equivalent volume diameter d_i of particles in each bin. The latter represents the diameter of a volume-equivalent sphere. Further, $i = 1, \ldots, n$ is the number of size bins used and $d_1 > d_2 > \ldots d_n$ for convenience. Then, the macroporosity ϕ_{Macro} can be expressed as

$$\phi_{Macro} = f(X_1, \ldots, X_n; d_1, \ldots, d_n; \phi_1, \ldots, \phi_n). \tag{6}$$

Note that the equivalent volume diameter d_i of particles is not strictly identical to the mean horizontal diameter as defined by Michikami et al. (2019), but as the observed boulder axes ratios on Ryugu change only little as a function of horizontal diameter, the shape factor relating horizontal diameter to the equivalent volume diameter d_i is close to constant. It can thus be factored out for the mixing model below and has a negligible effect on the Bond number.

The above formulation holds if particle sphericity is independent of particle size, which is the assumption made in the following and consistent with results obtained for Ryugu (Michikami et al., 2019). However, we note for completeness that the method to estimate macroporosity used here can be generalized to arbitrary sphericity-size relations $\Psi(d)$ by introducing the equivalent packing diameter d_p, which then accounts for particle shape effects, i.e., mixing of particles that have different sphericities at different sizes. Then, the equivalent volume diameter d in Eq. 6 needs to be replaced by the equivalent packing diameter d_p, which is related to the observed equivalent volume diameter d through sphericity $\Psi(d)$ by (Yu & Zou, 1998)

$$\frac{d}{d_p} = \Psi(d)^{2.785} e^{2.946(1-\Psi(d))} \tag{7}$$

The specific volume, i.e., the volume per unit mass finally attained by the mixture is governed by intermediate-sized particles, as the addition of unmixing components will not change the packing state (Yu & Zou (1998), also compare Fig. 1). Specific volume V_i and porosity ϕ_i are related by

$$V_i = \frac{1}{1 - \phi_i} \tag{8}$$

and while the size-bin number i of the controlling mixture is not known a priori, the specific volume $\tilde{V}_i$ of the particular packing can in general be expressed as

$$\tilde{V}_i = \sum_{j=1}^{i-1}[V_j - (V_j - 1)g(d_i, d_j)]X_j + V_i X_i + \sum_{j=i+1}^{n}[V_j(1 - f(d_i, d_j)]X_j \tag{9}$$

where small particles have indices $j = 1 \ldots i-1$ and large particles have indices $j = i{+}1 \ldots n$. The functions $f(d_i, d_j)$ and $g(d_i, d_j)$ are referred to as interaction functions between components i and j and were derived experimentally (Yu et al. (1997), Zou et al. (2011)). They are given by

$$f(d_i, d_j) = f(r_{ij}) = (1 - r_{ij})^{3.33} + 2.81 r_{ij}(1 - r_{ij})^{2.77} \quad \text{and} \tag{10}$$

$$g(d_i, d_j) = g(r_{ij}) = (1 - r_{ij})^{1.97} + 0.36 r_{ij}(1 - r_{ij})^{3.67} \tag{11}$$

and depend on the equivalent packing diameter size ratios r_{ij} between small and large particles of the two components. Parameters r_{ij} can be expressed as (Zou et al., 2011)

$$r_{ij} = (1 - x_{ij})R_{ij}^k + x_{ij} R_{ij} \tag{12}$$

where $R_{ij} = d_j/d_i$ is the small-to-large size ratio and $i < j$. The parameter k is 0.451 (Zou & Yu, 1996), and x_{ij} depends on the type of particle-particle interaction (Zou et al., 2011). It is given by

$$x_{ij} = \begin{cases} 1 & d_j \geq d_{cri} \\ 0 & d_i \leq d_{cri} \\ 1 - 1.543 \cdot e^{-0.697 d_i/d_{cri}} & d_j \leq d_{cri} \leq d_i \end{cases} \tag{13}$$

In the above equation, the critical particle diameter d_{cri} divides fine and coarse particles, i.e., it is the particle diameter below which cohesion between particles starts to influence particle interactions. Under Earth gravity conditions, d_{cri} is close to 150 µm (Zou et al., 2011), but under micro-gravity conditions, cohesion can be relevant even for decimeter-sizes boulders (Scheeres et al., 2010; Kiuchi & Nakamura, 2015; Zou et al., 2011). Here, we define the critical diameter based on the Bond number B, i.e., the ratio between interparticle forces and the weight of the particles (Scheeres et al., 2010). Including effects of particle sphericity Ψ and roundness Ω, we define the Bond number as

$$B(d) = \frac{1.1 \cdot 10^{17} A \Psi \Omega}{\rho g (d/2)^2} \tag{14}$$

where d is particle diameter, $A = 4.1 \cdot 10^{-20}$ J is the Hamaker constant (valid for olivine in high vacuum, Perko et al. (2001)), and $g = 0.9825 \cdot 10^{-4}$ m s^{-2} is volume averaged

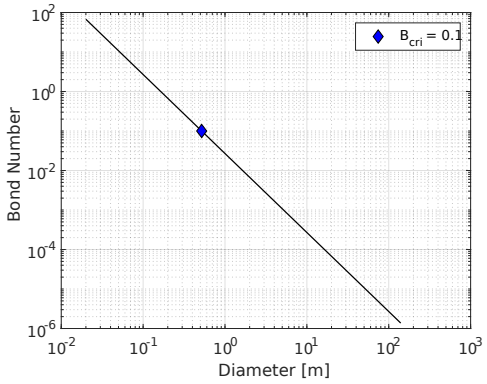

Figure 3. Bond number, i.e., the ratio between interparticle forces and particle weight, as a function of particle diameter, assuming parameters as appropriate for Ryugu. The diameter corresponding to a critical Bond number of $B_{cri} = 0.1$ is indicated.

gravity. We choose boulder bulk density $\rho = 1420$ kg m^{-3} to match a macroporosity of 16 % and a bulk density of 1190 kg m^{-3} (Watanabe et al., 2019) for consistency. Furthermore, we choose a particle roundness Ω of 0.24, as appropriate for angular to subangular particles (Powers, 1953).

The resulting Bond number for parameters appropriate for Ryugu is shown in Fig. 3 as a function of particle diameter. The critical diameter d_{cri} corresponding to a critical Bond number $B_{cri} = 0.1$ is indicated in blue and has been calculated using Eq. 14. We use $B_{cri} = 0.1$ as a baseline, i.e., we assume that adhesion starts to have a noticeable effect on porosity once the interparticle forces exceed 10 % of the particle weight. For Ryugu, $B_{cri} = 0.1$ corresponds to $d_{cri} = 0.52$ m, but the influence of varying B_{cri} will also be discussed.

To evaluate Eq. 9, we first discretize the size range between $D_{\min} = 0.02$ m and $D_{\max} = 140$ m into $\log(D_{\max}/D_{\min})/\log(q)$ logarithmically spaced bins. We use a size factor of $q = 1.05$ from one bin to the next, resulting in a total of 182 size bins. Then, initial specific volumes V_i and therefore initial porosities ϕ_i in the individual size-bins need to be prescribed. While initial porosities of coarse monosized spherical particles generally vary between 0.42 for loose random packing and 0.36 for dense random packing (Scott, 1960), cohesive forces between small particles can considerably increase porosities (Scheeres et al., 2010; Kiuchi & Nakamura, 2015). We use the empirical relation (Ki-

uchi & Nakamura, 2015; Kiuchi & Nakamura, 2015)

$$\phi_i = \phi_0 + (1 - \phi_0)e^{-\alpha B(d_i)^{-\gamma}} \tag{15}$$

to determine initial porosity, where ϕ_0 is the porosity of the non-cohesive particles and we choose $\phi_0 = 0.395$ as appropriate for intermediate packing densities. Note that we here implicitly assume initial porosities as appropriate for spherical particles, as for the relevant range of observed sphericities the influence of deviations from an ideal spherical shape on initial porosity is negligible (Zou & Yu, 1996). In Eq. 15, $B(d_i)$ is the Bond number (Eq. 14) at particle diameter d_i and the constants $\alpha = 2.414$ and $\gamma = 0.1985$ have been derived from a new fit to the data of Kiuchi & Nakamura (2015). Finally, the specific volume occupied by the mixture is obtained by calculating the maximum of all specific volumes for the different controlling mixture sizes and

$$V = \max\{\tilde{V}_1, \ldots, \tilde{V}_n\} \tag{16}$$

Mixture macroporosity is then given by $\phi_{Macro} = 1 - 1/V$.

2.3 Average Grain Density

While the main goal of the present paper is a determination of the macro-porosity of rubble-pile asteroid Ryugu, additional information on the asteroid's average grain density can be derived. As macroporosity ϕ_{Macro}, microporosity ϕ_{Micro}, and bulk density ρ_{Bulk} are related by

$$\phi_{\mathrm{Macro}} = 1 - \frac{1 - \phi_{\mathrm{Bulk}}}{1 - \phi_{\mathrm{Micro}}} \tag{17}$$

information on grain density ρ_{Grain} can be extracted from

$$\phi_{\mathrm{Bulk}} = 1 - \frac{\rho_{\mathrm{Bulk}}}{\rho_{\mathrm{Grain}}} \tag{18}$$

Eq. 18 requires the macroporosity, microporosity, and bulk density to be known. While the bulk density of Ryugu was estimated to be 1190±20 kg m^{-3} (Watanabe et al., 2019), the boulders' microporosity cannot currently be unambiguously constrained due to the difficulties associated with extrapolating meteorite thermal conductivities to porosities in excess of 20 % (Grott et al., 2019; Macke et al., 2011). However, end-member models (Flynn et al., 2018; Henke et al., 2016) suggest microporosities ϕ_{Micro} either between 28 to 35 % or between 41 to 55 % for Ryugu's dark and rugged boulders (Grott

et al., 2017, 2019) which comprise the vast majority of all boulders observed on the surface (Sugita et al., 2019). We will use Monte-Carlo simulations to propagate these uncertainties to the determination of Ryugu's grain density, while simultaneously taking the uncertainty associated with Ryugu's macroporosity as derived from the linear mixing theory (Sec. 2.2) into account.

3 Results

Given the parameterization of the size-frequency distribution (Eq. 1) for the boulders observed on the surface of Ryugu, and assuming the distribution also applies to the interior, we have first calculated the corresponding volume frequency distribution using Eq. 2. Given roundness Ω, Hamaker constant A, particle bulk density ρ, and volume average gravity g (see Eq. 14), we then varied the initial porosity ϕ_i in each size bin using a Gaussian distribution centered around 39.5 % with standard deviation of 3 %. In addition, particle sphericity was varied using a Gaussian distribution centered around 0.85 with standard deviation of 0.06, and 10^6 draws from these distributions were used in a Monte-Carlo simulation to calculate the resulting macroporosity according to Eq. 16.

Results of the calculation are shown in the left hand panel of Fig. 4, where a histogram of the obtained macroporosities ϕ_M is shown. The range of macroporosities obtained in the calculations is $\phi_M = 16.2 \pm 2.6$ %, and thus considerably smaller than porosities of monodisperse packings. This is not surprising given the broad particle size distribution observed on the surface of Ryugu. Here and in the following, stated errorbars refer to one standard deviation and thus represent 68 % confidence intervals.

Given the range of macroporosities derived above as well as estimates for the boulder microporosities derived from in-situ thermal inertia measurements (Grott et al., 2019), we calculated the range of grain densities compatible with the observed bulk porosity of Ryugu (Watanabe et al., 2019) using Eq. 17 and 18. We applied two endmember models for the microporosity ϕ_{Micro}: for the first model (Flynn et al., 2018) 41 % $< \phi_{Micro} <$ 55 %, while for the second model (Henke et al., 2016) 28 % $< \phi_{Micro} <$ 34 %. In the 10^6 Monte-Carlo simulations performed, we varied microporosity using uniformly distributed random numbers between 41 % and 55 % as well as 28 % and 34 %, respectively. Furthermore, we varied bulk density using a Gaussian distribution centered around 1190

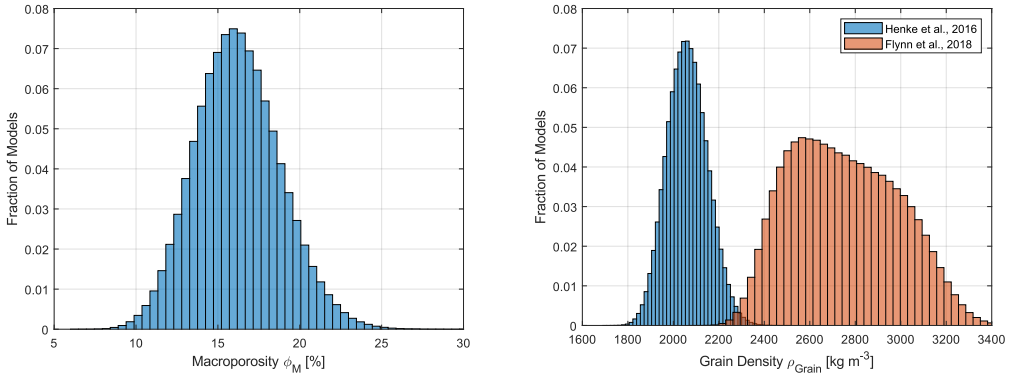

Figure 4. Left: Histogram of macroporosities ϕ_M obtained using Monte-Carlo simulations. Right: Ryugu grain densities derived from a second set of Monte-Carlo calculations (see text for details). The bimodal distribution results from the uncertainty of microporosity for Ryugu's boulders (Grott et al., 2019), and two end-member models for the microporosity have been assumed.

kg m^{-3} with a standard deviation of 20 kg m^{-3} (Watanabe et al., 2019) and macroporosity using a Gaussian distribution centered around 16.2% with a standard deviation of 2.6 %.

Results of the calculation are shown in the right hand panel of Fig. 4, where the resulting histograms for the grain densities ρ_{Grain} are shown for the two endmember models. Owing to the two different models used to estimate boulder microporosity, two separate peaks are obtained for the distribution of grain densities. For the model of Flynn et al. (2018), we find grain densities of $\rho_{Grain} = 2751 \pm 236$ kg m^{-3}, whereas the model of Henke et al. (2016) results in $\rho_{Grain} = 2062 \pm 89$ kg m^{-3}. As expected, higher microporosities (Flynn et al., 2018) yield larger grain densities and vice versa to satisfy the constraint posed by Ryugu's bulk density.

Results of a systematic study of the influence of critical Bond number B_{cri} and lower diameter cutoff sizes $D_{\min}$ on the obtained macroporosities ϕ_{Macro} are shown in Fig. 5. Here, the size-frequency distribution of boulders has been approximated by a power law with exponent p to facilitate a comparison of Ryugu with other rubble pile asteroids. For smaller power law exponents, the size-frequency distribution is shallower as compared to distributions with larger p, and as a result, such distributions represent surfaces with a higher ratio of large particles.

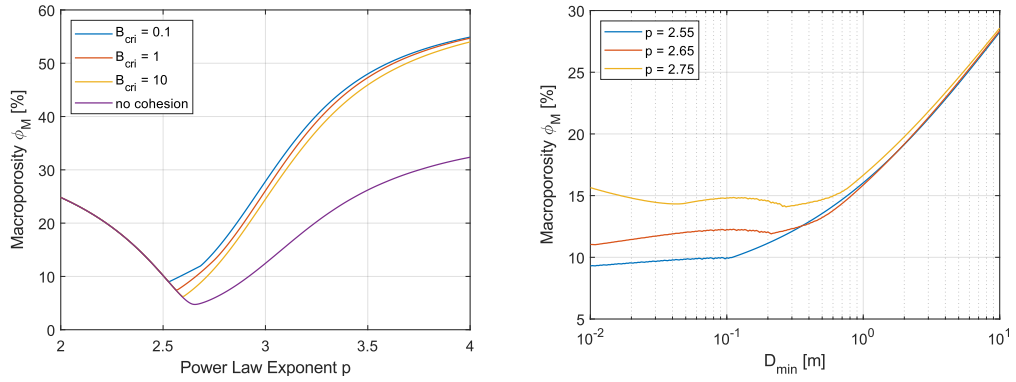

Figure 5. Left: Macroporosity ϕ_{Macro} (porosity caused by void spaces in-between particles) as a function of the power law exponent of the underlying size-frequency distribution and critical Bond number B_{cri}. For comparison, results obtained neglecting cohesion between particles are also shown. Right: Macroporosity ϕ_{Macro} as a function of lower cutoff size D_{min} for three different power law exponents p. For reference, the power law exponent for Ryugu as derived from the observed surface boulder size-frequency distribution is $p = 2.65$ on average (Michikami et al., 2019).

In general, the macroporosities ϕ_{Macro} obtained using the above mixing theory show a distinct minimum at intermediate power law exponents p, whereas distributions which have too many small or too many large particles result in unfavorable mixing and larger ϕ_{Macro} are obtained. This minimum around $p = 2.5$ is known as the Fuller parabola in the engineering literature and has long been known as the optimum packing size distribution for spherical particles (Fuller & Thompson, 1907). Results obtained varying the critical Bond number are shown in the left panel of Fig. 5, where the critical Bond number parametrizes the particle size below which interparticle forces result in significant cohesion. As expected, low critical Bond numbers, corresponding to larger contributions from cohesive particles, result in larger macroporosities. However, the overall effect is small and in the few percent range. The low critical Bond number of 0.1 adopted above therefore results in a conservative upper limit on macroporosity. It is also worth noting that results obtained using a power law distribution with $p = 2.65$ are lower than those obtained using the Weibull representation of the data by 4-5 %, such that results obtained using global power law fits must be interpreted with caution. For comparison, results obtained neglecting cohesion are also shown in the left panel of Fig. 5, and macroporosity approaches a limit of 39.5 % (compare Eq. 15) for large p (not shown).

The influence of varying the lower cutoff diameter $D_{\min}$ of the size-frequency distribution on the obtained macroporosity ϕ_{Macro} is shown in the right panel of Fig. 5, where ϕ_{Macro} is shown as a function of $D_{\min}$ for three power law exponents p. In the calculations, a critical Bond number of $B_{cri} = 0.1$ has been assumed. While the minimum macroporosity that can be achieved by the packing is close to constant for small D_{min}, predicted macroporosity drastically increases for cutoff diameters larger than a few decimeters. In this case, unfavorable mixing is a result of the sparsity of smaller rocks to fill the gaps between larger blocks. These results indicate that image data with centimeter resolution are necessary to properly characterize the packing state of rubble pile asteroids, and that results presented above are largely independent of the cutoff size of $D_{\min} = 0.02$ m imposed by the image data available for Ryugu.

4 Discussion and Conclusions

In the present paper, we have used semi-empirical models for the porosity of multi-component mixtures to estimate the macroporosity of Cb-type asteroid (162173) Ryugu based on the observed size-frequency distribution of boulders on the asteroid's surface and the assumption that the surface distribution of boulders is representative for the bulk asteroid. Using the concept of controlling mixtures (Yu & Standish, 1991; Yu & Zou, 1998; Zou et al., 2011), we estimated the macroporosity of Ryugu to be $\phi_M = 16.2 \pm 2.6$ %. Based on estimates of boulder microporosity, we furthermore constrained the average grain density of Ryugu's to $\rho_{Grain} = 2751 \pm 236$ kg m^{-3} or $\rho_{Grain} = 2062 \pm 89$ kg m^{-3}, depending on the microporosity model used. While the applied model takes cohesion between particles into account, results obtained for Ryugu do not significantly depend on the chosen critical Bond number. This is a result of the low volume fraction of small cohesive particles, and models disregarding cohesion result in similar macroporosities as those reported here.

The cratering experiment performed by Hayabusa2's small carry-on impactor resulted in the formation of a crater in the gravity-dominated regime (Arakawa et al., 2020), indicating that particle cohesion played a minor role in the crater formation process. On the other hand, particles with diameters well below 0.2 m were observed in the ejecta, which, according to Eq. 14, have Bond numbers close to unity and should therefore interact cohesively. This apparent discrepancy could be resolved if either the Bond number has been overestimated here, which could for example be caused by neglecting small

surface asperities or the presence of adsorbed gases, or if small particles are not volumetrically dominant inside Ryugu. The latter is indicated by the shallow particle size distribution for particles smaller than 1 m on the surface (Sugita et al., 2019; Michikami et al., 2019) and inside the artificial crater (Arakawa et al. (2020), Fig. S5), where the particle size distribution shows a power law exponent $p \sim 2$ (also compare the volume-size distribution on the right hand side of Fig. 2). In any case, results of the cratering experiment indicate that cohesion might have a small influence on the packing state, and the above macroporosities should therefore be regarded as upper limits. However, cohesion may become significant for rubble pile asteroids with a steep particle size distribution, e.g., power-laws with $p > 3$, where - in contrast to Ryugu - the mixture is dominated by a high volume fraction of very small particles.

Although a full analysis using empirical fits of the cumulative boulder size-frequency distribution of other small bodies has not been performed here, macroporosity results can be qualitatively compared by considering the power law exponents of their respective size distributions and assuming similar size cutoffs $D_{\min}$ and $D_{\max}$. The former have been widely used to describe size distributions in the literature, and values of $p = 2.91 \pm 0.3$ and $p = 3.52 \pm 0.20$ have been obtained for Bennu (Lauretta et al., 2019) and Itokawa (Michikami et al., 2008; Mazrouei et al., 2014; Michikami et al., 2019), respectively. Assuming $B_{cri} = 1$ to obtain a best estimate, these correspond to macroporosities between 8.5 and 37 % for Bennu and 42 to 51.5 % for Itokawa. Assuming average grain densities of 2600 kg m^{-3}, Bennu's low bulk density of 1190±13 kg m^{-3} (Lauretta et al., 2019) implies a bulk porosity of 54 %, indicating significant microporosity. For Itokawa, average grain density has been estimated based on the modal abundance of minerals in the returned samples, and densities of 3400 kg m^{-3} have been obtained (Tsuchiyama et al., 2011, 2014). This implies a bulk porosity of 39±6 % (Abe et al., 2006; Fujiwara et al., 2006; Tsuchiyama et al., 2011), consistent with the results obtained from the mixing theory. For Eros, the power law exponent of $p = 3.31 \pm 0.06$ (Thomas et al., 2001) implies macroporosities of 39 - 43 %. This is inconsistent with the inferred bulk porosity of Eros, which is estimated to be 21-33 % (Yeomans et al., 2000; Wilkison et al., 2002). However, although Eros is a heavily fractured body, there is little evidence that it was ever catastrophically disrupted and later reaccumulated into a rubble pile (Wilkison et al., 2002), such that the theory presented here can probably not be be applied.

Results for Ryugu have been obtained assuming minimum and maximum particle sizes of 0.02 m and 140 m, respectively, and these results are robust with respect to the cut-off at small particle sizes $D_{\min}$. Only shifting the cut-off $D_{\min}$ to values larger than 0.30 m has a noticeable effect on the macroporosity. The upper cut-off size $D_{\max}$ was chosen to correspond to the Otohime boulder, which is the largest boulder observed on Ryugu's surface. However, boulders larger than Otohime could potentially reside in Ryugu's interior, which would decrease the obtained macroporosity through a filling of void spaces. Reasonable upper limits on monolith sizes are 200 m, as derived from observations of fast rotators in the asteroid population (Pravec & Harris, 2000) and the catastrophic disruption threshold for disruption of asteroids (Benz & Asphaug, 1999; Jutzi et al., 2010). Assuming $D_{\max} = 200$ m reduces ϕ_{Macro} to 15 %.

One way to increase macroporosity in the above models would be an increased initial porosity in each size bin, which may for example be caused by mechanical interlocking of particles due to particle angularity. For a random loose packing, non-cohesive initial porosity can increase from ∼42 % for smooth frictionless particles to ∼44 % for very rough particles (Onoda & Liniger, 1990; Jerkins et al., 2008). In the frame of the applied mixing model, this effect is taken into account in the chosen initial porosity (Eq. 15), and shifting the applied Gaussian distribution in the performed Monte-Carlo simulations by 2 % results in slightly increased macroporosities of 18.0±3 %. Therefore, while roughness and particle interlocking can increase macroporosity, this is likely not a significant effect.

While the obtained macroporosity may appear to be relatively low, a significant reduction with respect to the porosity of random close packings of monodisperse spheres can be expected. Even binary mixtures of particles can be arranged in packing states with porosities of 15-20 % (Yu & Standish, 1991; Yu et al., 1992), such that it should not be surprising to achieve similar packing densities with the broad size distributions used here. Ternary mixtures can achieve $\phi_{Macro} < 10$ % (Yu & Standish, 1991), and while most common loose or compact granular materials have macroporosities between 0.3 and 0.5, almost any degree of macroporosity between 10 and 90 % can be obtained for non-uniform angular particles (Dullien, 1991). Experimentally, macroporosities down to 10 % have been produced in the lab (Latham et al., 2002). Therefore, the macroporosity of Ryugu obtained here falls within a reasonable range, and Ryugu's high bulk porosity is a direct consequence of the very large microporosity of Ryugu's boulders.

The average grain densities obtained here are much lower than typical grain densities of ordinary chondrites, which range from 3520 to 3710 kg m^{-3} (Flynn et al., 2018), and also lower than those of most carbonaceous chondrites, which typically have grain densities in excess of 3360 kg m^{-3} (Flynn et al., 2018). Only the CM and CI sub-classes show lower grain densities, and $\rho_{CM,Grain} = 2960 \pm 40$ kg m^{-3} while $\rho_{CI,Grain} = 2420$ kg m^{-3} (Consolmagno et al., 2008; Macke et al., 2011; Flynn et al., 2018). The Tagish Lake meteorite, an ungrouped carbonaceous chondrite, exhibits similar grain densities in the range between 2430 and 2840 kg m^{-3} (Ralchenko et al., 2014). While the larger grain densities of 2751 ± 236 kg m^{-3} are consistent with the CM, CI, and Tagish Lake results, the lower densities of 2062 ± 89 kg m^{-3} are inconsistent with those of known meteorite samples.

Estimates of grain densities discussed above indicate that extrapolating boulder porosities as a function of thermal conductivity using the model by Flynn et al. (2018) is preferred to extrapolations using the model by Henke et al. (2016). In addition, laboratory measurements of thermal conductivity (Hamm et al., 2019) using the UTPS Tagish Lake meteorite simulant (Miyamoto et al., 2018) provide further evidence of high boulder microporosity. The UTPS simulant has a grain density of 2813 kg m^{-3} and a porosity of 47.5 %, while thermal conductivity was determined to be similar to that of Ryugu's rugged boulders (Hamm et al., 2019). It therefore seems likely that boulder porosity on Ryugu falls within the high range determined by Grott et al. (2019), but more laboratory measurements of thermal conductivity at high porosity are needed to confirm these results and reduce uncertainties. If grain densities are indeed of the order of 2750 kg m^{-3}, Ryugu's bulk porosity is estimated to be 57 % (cp. Eq. 18).

It is noted that close-up images have revealed that many boulders on Ryugu and Bennu exhibit morphologic properties consistent with a brecciated structure (Sugita et al., 2019; Walsh et al., 2019). Breccia would have much larger microporosities than pristine rocks, consistent with the large microporosities preferred here. Furthermore, the presence of breccia on Ryugu and Bennu is consistent with the fact that many carbonaceous chondrites and, in particular, all CM and CI meteorites found on Earth are known to be brecciated (Bischoff et al., 2006). However, it remains to be investigated if brecciation is the main mechanism providing microporosity, or whether the boulder's highly porous structure is a result of the formation mechanisms acting in Ryugu's parent body (Neumann et al., 2014, 2015).

If microporosity in typical carbonaceous asteroids is as high as predicted here for Ryugu, macroporosities of rubble pile asteroids may have been systematically overestimated in the past (e.g., Consolmagno et al., 2008). Macroporosities have been estimated based on measurements of asteroid bulk density and porosities of meteorite samples, the latter of which could have been underestimated compared to values for actual carbonaceous material on asteroids derived from in-situ measurements (Grott et al., 2019). This bias could be the result of filtering by the Earth's atmosphere, as only the strongest, densest carbonaceous meteoroids would survive atmospheric entry, while weaker samples would break up (Popova et al., 2011). This could explain the absence of high porosity samples in our meteorite collections, where the most porous sample reported to date is the Tagish Lake meteorite, which shows porosities in the range from 26 to 36 % (Ralchenko et al., 2014). The samples to be returned from Ryugu by the Hayabusa2 mission will provide crucial information on this issue.

Results presented here assume that the size-frequency distribution observed on the surface of Ryugu is representative for the entire asteroid, but it has been argued that particle size sorting may take place during rubble pile re-accretion, with larger blocks accreting first and thus in the center (Britt & Consolmagno S.J., 2001). On the other hand, seismic shaking and the Brazil Nut Effect could lead to an overrepresentation of large boulders on the surface (Maurel et al., 2017), as particle motion could for example be induced by seismic shaking. This topic can be addressed once average grain density and possibly also microporosity have been determined from the returned samples, as has been done for Itokawa (Tsuchiyama et al., 2011). Then, Ryugu's macroporosity can be derived given the measured bulk density (Watanabe et al., 2019). Any significant deviation from the macroporosity value calculated here will indicate a non-homogeneous boulder size distribution in the bulk volume of the asteroid.

Acknowledgments

PM. acknowledges funding support from the French space agency CNES, from the European Union's Horizon 2020 research and innovation programme under grant agreement No 870377 (project NEO-MAPP), and from Academies of Excellence: Complex systems and Space, environment, risk and resilience, part of the IDEX JEDI of the Université Côte d'Azur. S.S. acknowledges funding from the JSPS Core-to-Core Program 'International Network of Planetary Sciences.'. W.N. acknowledges support by Klaus Tschira

Stiftung. Data has been made available at `https://doi.org/10.6084/m9.figshare.c.4964363.v1`.

References

Abe, S., Mukai, T., Hirata, N., Barnouin-Jha, O., Cheng, A., Demura, H., ... Yoshikawa, M. (2006). Mass and local topography measurements of itokawa by hayabusa. *Science*, *312*(5778), 1344–1347. doi: 10.1126/science.1126272

Arakawa, M., Saiki, T., Wada, K., Ogawa, K., Kadono, T., Shirai, K., ... Miura, A. (2020). An artificial impact on the asteroid 162173 Ryugu formed a crater in the gravity-dominated regime. *Science*, *367*, aaz1701. doi: 10.1126/science.aaz1701

Benz, W., & Asphaug, E. (1999). Catastrophic disruptions revisited. *Icarus*, *142*(1), 5 - 20. doi: 10.1006/icar.1999.6204

Bischoff, A., Scott, E. R. D., Metzler, K., & Goodrich, C. A. (2006). Nature and origins of meteoritic breccias. *Meteorites and the early solar system II*, 679-712.

Britt, D. T., & Consolmagno S.J., G. J. (2001). Modeling the Structure of High Porosity Asteroids. *Icarus*, *152*(1), 134-139. doi: 10.1006/icar.2001.6628

Britt, D. T., Yeomans, D., Housen, K., & Consolmagno, G. (2002). Asteroid density, porosity, and structure. In (p. 485-500). in: Asteroids III, W. F. Bottke Jr., A. Cellino, P. Paolicchi, and R. P. Binzel (eds), University of Arizona Press, Tucson.

Brown, W. K., & Wohletz, K. H. (1995). Derivation of the weibull distribution based on physical principles and its connection to the rosin-–rammler and lognormal distributions. *Journal of Applied Physics*, *78*(4), 2758-2763. doi: 10.1063/1.360073

Consolmagno, G. J., Britt, D. T., & Macke, R. J. (2008). The significance of meteorite density and porosity. *Chemie der Erde-Geochemistry*, *68*(1), 1–29.

Dullien, F. A. L. (1991). *Porous media - fluid transport and pore structure (second edition)* (Second Edition ed.). San Diego: San Diego, Academic Press. doi: 10.1016/B978-0-12-223651-8.50006-7

Durda, D. D., Bagatin, A. C., Alemañ, R. A., Flynn, G. J., Strait, M. M., Clayton, A. N., & Patmore, E. B. (2015). The shapes of fragments from catastrophic disruption events: Effects of target shape and impact speed. *Planetary and Space Science*, *107*, 77 - 83. (VIII Workshop on Catastrophic Disruption in the Solar System) doi: https://doi.org/10.1016/j.pss.2014.10.006

Flynn, G. J., Consolmagno, G. J., Brown, P., & Macke, R. J. (2018). Physical properties of the stone meteorites: Implications for the properties of their parent bodies. *Chemie der Erde / Geochemistry*, *78*(3), 269-298. doi: 10.1016/j.chemer.2017.04.002

Fujiwara, A., Kawaguchi, J., Yeomans, D. K., & et al. (2006). The Rubble-Pile Asteroid Itokawa as Observed by Hayabusa. *Science*, *312*(5778), 1330-1334. doi: 10.1126/science.1125841

Fuller, W. B., & Thompson, S. E. (1907). The laws of proportioning concrete. *Trans. Am. Soc. Civ. Eng.*, *59*(2), 67-143.

Graton, L. C., & Fraser, H. J. (1935, December). Systematic Packing of Spheres: With Particular Relation to Porosity and Permeability. *Journal of Geology*, *43*(8), 785-909. doi: 10.1086/624386

Grott, M., Knollenberg, J., Borgs, B., Hänschke, F., Kessler, E., Helbert, J., ... Müller, N. (2017). The MASCOT Radiometer MARA for the Hayabusa 2 Mission. *Space Science Reviews*, *208*(1-4), 413-431. doi: 10.1007/s11214-016-0272-1

Grott, M., Knollenberg, J., Hamm, M., Ogawa, K., Jaumann, R., Otto, K. A., ... Moussi-Soffys, A. (2019). Low thermal conductivity boulder with high porosity identified on C-type asteroid (162173) Ryugu. *Nature Astronomy*, 406. doi: 10.1038/s41550-019-0832-x

Hamm, M., Grott, M., Knollenberg, J., Miyamoto, H., Biele, J., Hagermann, A., ... Zolensky, M. (2019). Thermal Conductivity and Porosity of Ryugu's Boulders from In-Situ Measurements of MARA - the MASCOT Radiometer. In *Lunar and planetary science conference* (p. 1373).

Henke, S., Gail, H.-P., & Trieloff, M. (2016). Thermal evolution and sintering of chondritic planetesimals. III. Modelling the heat conductivity of porous chondrite material. *Astronomy and Astrophysics*, *589*, A41. doi: 10.1051/0004-6361/201527687

Jerkins, M., Schröter, M., Swinney, H., Senden, T. J., Saadatfar, M., & Aste, T. (2008). Onset of Mechanical Stability in Random Packings of Frictional Spheres. *Phys. Rev. Lett.*, *101*(1), 018301. doi: 10.1103/PhysRevLett.101.018301

Jutzi, M., Michel, P., Benz, W., & Richardson, D. (2010). Fragment properties at the catastrophic disruption threshold: The effect of the parent body's internal structure. *Icarus*, *207*(1), 54 - 65. doi: 10.1016/j.icarus.2009.11.016

Kitazato, K., Milliken, R. E., & Iwata, e. a., T. (2019). The surface composition of asteroid 162173 ryugu from hayabusa2 near-infrared spectroscopy. *Science*, *364*(6437), 272–275. doi: 10.1126/science.aav7432

Kiuchi, M., & Nakamura, A. M. (2015). Corrigendum to "Relationship between regolith particle size and porosity on small bodies" [Icarus 239 (2014) 291-293]. *Icarus*, *248*, 221-221. doi: 10.1016/j.icarus.2014.10.039

Kiuchi, M., & Nakamura, A. M. (2015). Corrigendum to"relationship between regolith particle size and porosity on small bodies"[icarus 239 (2014) 291-293]. *Icarus*, *248*, 221-221.

Krumbein, W. C. (1941). Measurement and geological significance of shape and roundness of sedimentary particles. *Journal of Sedimentary Petrology*, *11*, 64-72.

Latham, J. P., Munjiza, A., & Lu, Y. (2002). On the prediction of void porosity and packing of rock particulates. *Powder Technology*, *125*, 10-27. doi: 10.1016/S0032-5910(01)00493-4

Lauretta, D. S., Dellagiustina, D. N., Bennett, C. A., & et al. (2019). The unexpected surface of asteroid (101955) Bennu. *Nature*, *568*(7750), 55-60. doi: 10.1038/s41586-019-1033-6

Macke, R. J., Consolmagno, G. J., & Britt, D. T. (2011). Density, porosity, and magnetic susceptibility of carbonaceous chondrites. *Meteorit. Planet. Sci.*, *46*, 1842–1862.

Maurel, C., Ballouz, R.-L., Richardson, D. C., Michel, P., & Schwartz, S. R. (2017). Numerical simulations of oscillation-driven regolith motion: Brazil-nut effect. *Monthly Notices of the Royal Astronomical Society*, *464*(3), 2866-2881. doi: 10.1093/mnras/stw2641

Mazrouei, S., Daly, M. G., Barnouin, O. S., Ernst, C. M., & DeSouza, I. (2014). Block distributions on Itokawa. *Icarus*, *229*, 181-189. doi: 10.1016/j.icarus.2013.11.010

Michel, P., Ballouz, R.-L., Barnouin, O., Jutzi, M., Walsh, K., May, B., ... Lauretta, D. (2020). Collisional formation of top-shaped asteroids and implications for the origins of ryugu and bennu. *Nature Communications*.

Michel, P., & Richardson, D. C. (2013). Collision and gravitational reaccumulation: Possible formation mechanism of the asteroid itokawa. *Astron. Astrophys.*, *554*, L1-L4.

Michikami, T., Hagermann, A., Kadokawa, T., Yoshida, A., Shimada, A., Hasegawa, S., & Tsuchiyama, A. (2016). Fragment shapes in impact experiments ranging from cratering to catastrophic disruption. *Icarus*, *264*, 316-330. doi: 10.1016/j.icarus.2015.09.038

Michikami, T., Honda, C., Miyamoto, H., & et al. (2019). Boulder size and shape distributions on asteroid ryugu. *Icarus*, *331*, 179 - 191. doi: https://doi.org/10.1016/j.icarus.2019.05.019

Michikami, T., Nakamura, A. M., Hirata, N., Gaskell, R. W., Nakamura, R., Honda, T., ... Miyamoto, H. (2008). Size-frequency statistics of boulders on global surface of asteroid 25143 Itokawa. *Earth, Planets, and Space*, *60*, 13-20. doi: 10.1186/BF03352757

Miyamoto, H., Niihara, T., Wada, K., Ogawa, K., Baresi, N., Abell, P., ... Nakamura, T. (2018). Phobos Environment Model and Regolith Simulant for MMX Mission. In *Lunar and planetary science conference* (p. 1882).

Nakamura, A., & Fujiwara, A. (1991). Velocity distribution of fragments formed in a simulated collisional disruption. *Icarus*, *92*(1), 132-146. doi: 10.1016/0019-1035(91)90040-Z

Neumann, W., Breuer, D., & Spohn, T. (2014). Modelling of compaction in planetesimals. *A&A*, *567*, A120. doi: 10.1051/0004-6361/201423648

Neumann, W., Breuer, D., & Spohn, T. (2015). Modelling the internal structure of Ceres: Coupling of accretion with compaction by creep and implications for the water-rock differentiation. *A&A*, *584*, A117. doi: 10.1051/0004-6361/201527083

Okada, T., Fukuhara, T., Tanaka, S., & et al. (2020). Highly porous nature of a primitive asteroid revealed by thermal imaging. *Natureh*, *579*, 518–52. doi: 10.1038/s41586-020-2102-6

Onoda, G. Y., & Liniger, E. G. (1990). Random loose packings of uniform spheres and the dilatancy onset. *Phys. Rev. Lett.*, *64*(22), 2727-2730. doi: 10.1103/PhysRevLett.64.2727

Perko, H., Nelson, J., & Sadeh, W. (2001). Surface cleanliness effect on lunar soil shear strength. *J. Geotech. Geoenviron. Eng.*, *127*(4), 371-383. doi: 10.1061/(asce)1090-0241(2001)127:4(371)

Popova, O., Borovicka, J., Hartmann, W. K., Spurny, P., Gnos, E., Nemtchinov, I., & Trigo-Rodriguiz, J. M. (2011). Very low strengths of interplanetary meteoroids

and small asteroids. *Meteoritics & Planetary Science*, *46*(10), 1525-1550. doi: 10.1111/j.1945-5100.2011.01247.x

Powers, M. C. (1953). A new roundness scale for sedimentary particles. *J. Sediment. Res.*, *23*(2), 117-119. doi: 10.1306/D4269567-2B26-11D7-8648000102C1865D

Pravec, P., & Harris, A. W. (2000). Fast and Slow Rotation of Asteroids. *Icarus*, *148*, 12-20. doi: 10.1006/icar.2000.6482

Ralchenko, M., Britt, D. T., Samson, C., Herd, C. D. K., Herd, R. K., & McCausland, P. J. A. (2014). Bulk Physical Properties of the Tagish Lake Meteorite Frozen Pristine Fragments. In *Lunar plan. sci. conf.* (p. 1021).

Riley, N. (1941). Projection sphericity. *J. Sediment. Petrol.*, *11*, 94-95.

Rosin, P., & Rammler, E. (1933). The laws governing the fineness of powdered coal. *Journal of the Institute of Fuel*, *7*, 29–36.

Scheeres, D. J., Hartzell, C. M., Sánchez, P., & Swift, M. (2010). Scaling forces to asteroid surfaces: The role of cohesion. *Icarus*, *210*(2), 968-984. doi: 10.1016/j.icarus.2010.07.009

Scott, G. D. (1960). Packing of spheres: Packing of equal spheres. *Nature*, *188*, 908–909. doi: 10.1038/188908a0

Sugita, S., Honda, R., Morota, T., & et al. (2019). The geomorphology, color, and thermal properties of ryugu: Implications for parent-body processes. *Science*, *364*(6437). doi: 10.1126/science.aaw0422

Thomas, P. C., Veverka, J., Robinson, M. S., & Murchie, S. (2001). Shoemaker crater as the source of most ejecta blocks on the asteroid 433 Eros. *Nature*, *413*(6854), 394-396. doi: 10.1038/35096513

Tsuchiyama, A., Uesugi, M., Matsushima, T., Michikami, T., Kadono, T., Nakamura, T., ... Kawaguchi, J. (2011). Three-dimensional structure of hayabusa samples: Origin and evolution of itokawa regolith. *Science*, *333*(6046), 1125–1128. doi: 10.1126/science.1207807

Tsuchiyama, A., Uesugi, M., Uesugi, K., Nakano, T., Noguchi, R., Matsumoto, T., ... Fujimura, A. (2014). Three-dimensional microstructure of samples recovered from asteroid 25143 itokawa: Comparison with ll5 and ll6 chondrite particles. *Meteoritics & Planetary Science*, *49*(2), 172-187. doi: 10.1111/maps.12177

Wadell, H. (1932). Volume, Shape, and Roundness of Rock Particles. *Journal of Geology*, *40*(5), 443-451. doi: 10.1086/623964

Walsh, K. J., Jawin, E. R., Ballouz, R. L., Barnouin, O. S., Bierhaus, E. B., Connolly, H. C., ... Osiris-Rex Team (2019). Craters, boulders and regolith of (101955) Bennu indicative of an old and dynamic surface. *Nature Geoscience*, *12*(4), 242-246. doi: 10.1038/s41561-019-0326-6

Watanabe, S., Hirabayashi, M., Hirata, N., & et al. (2019). Hayabusa2 arrives at the carbonaceous asteroid 162173 ryugu—a spinning top–shaped rubble pile. *Science*, *364*(6437), 268–272. doi: 10.1126/science.aav8032

Weibull, W. (1951). A statistical distribution function of wide applicability. *J. Appl. Mech.-Trans. ASME*, *18 (3)*, 293–29.

Wilkison, S. L., Robinson, M. S., Thomas, P. C., Veverka, J., McCoy, T. J., Murchie, S. L., ... Yeomans, D. K. (2002). An estimate of eros's porosity and implications for internal structure. *Icarus*, *155*(1), 94 - 103. doi: https://doi.org/10.1006/icar.2001.6751

Wilson, L., Keil, K., & Love, S. J. (1999). The internal structures and densities of asteroids. *Meteoritics and Planetary Science*, *34*(3), 479-483. doi: 10.1111/j.1945-5100.1999.tb01355.x

Wingo, D. R. (1989). The left-truncated weibull distribution: theory and computation. *Statistical papers*, *30*(1), 39–48.

Yeomans, D. K., Antreasian, P. G., Barriot, J. P., Chesley, S. R., Dunham, D. W., Farquhar, R. W., ... Williams, B. G. (2000, September). Radio Science Results During the NEAR-Shoemaker Spacecraft Rendezvous with Eros. *Science*, *289*(5487), 2085-2088. doi: 10.1126/science.289.5487.2085

Yu, A. B., Bridgwater, J., & Burbidge, A. (1997). On the modelling of the packing of fine particles. *Powder Technology*, *92*(3), 185 - 194. doi: 10.1016/S0032-5910(97)03219-1

Yu, A. B., & Standish, N. (1991). Estimation of the porosity of particle mixtures by a linear-mixture packing model. *Industrial & Engineering Chemistry Research*, *30*(6), 1372-1385. doi: 10.1021/ie00054a045

Yu, A. B., & Zou, R. P. (1998). Prediction of the porosity of particle mixtures. *KONA Powder and Particle Journal*, *16*, 68-81. doi: 10.14356/kona.1998010

Yu, A. B., Zou, R. P., & Standish, N. (1992). Packing of ternary mixtures of non-spherical particles. *Journal of the American Ceramic Society*, *75*(10), 2765-2772. doi: 10.1111/j.1151-2916.1992.tb05502.x

Zou, R. P., Gan, M. L., & Yu, A. B. (2011). Prediction of the porosity of multi-component mixtures of cohesive and non-cohesive particles. *Chemical Engineering Science*, *66*(20), 4711-4721. doi: 10.1016/j.ces.2011.06.037

Zou, R. P., & Yu, A. B. (1996). Evaluation of the packing characteristics of mono-sized non-spherical particles. *Powder Technology*, *88*(1), 71 - 79. doi: https://doi.org/10.1016/0032-5910(96)03106-3